Int J Comput Vis
DOI 10.1007/s11263-014-0728-2

Affine Invariant Geometry for Non-rigid Shapes

Dan Raviv · Ron Kimmel

Received: 18 February 2012 / Accepted: 29 April 2014

Abstract Shape recognition deals with the study geometric structures. Modern surface processing methods can cope with non-rigidity—by measuring the lack of isometry, deal with similarity or scaling—by multiplying the Euclidean arc-length by the Gaussian curvature, and manage equi-affine transformations—by resorting to the special affine arc-length definition in classical equi-affine differential geometry. Here, we propose a computational framework that is invariant to the full affine group of transformations (similarity and equi-affine). Thus, by construction, it can handle non-rigid shapes. Technically, we add the similarity invariant property to an equi-affine invariant one and establish an affine invariant pseudo-metric. As an example, we show how diffusion geometry can encapsulate the proposed measure to provide robust signatures and other analysis tools for affine invariant surface matching and comparison.

1 Introduction

Differential invariants for planar shape matching and recognition were introduced to computer vision in the 1980's (Weiss 1988) and studied in the early 1990's (Bruckstein et al. 1992, 1993; Cohignac et al. 1994; Bruckstein and Netravali 1995; Calabi et al. 1998; Bruckstein and Shaked 1998), where global invariants were computed in a local manner to overcome numerical sensitivity of the differential forms. Scale space entered the game as a stabilizing mechanism, for example in Bruckstein et al. (1997), where locality was tuned by a scalar indicating how far one should depart from the point of interest. Along a different path, using a point matching oracle to reduce the number of derivatives, semi-differential signatures were proposed in Van Gool et al. (1992a,b), Moons et al. (1995), Pauwels et al. (1995), Carlsson et al. (1996). Non-local signatures, which are more sensitive to occlusions, were shown to perform favorably in holistic paradigms (Olver 1999, 2005; Brook et al. 2005; Ling and Jacobs 2005). At another end, image simplification through geometric invariant heat processes were introduced and experimented with during the late 1990's, (Sapiro 1993; Alvarez et al. 1993; Kimmel 1996). At the beginning of this century, scale space theories gave birth to the celebrated *scale invariant feature transform* (SIFT) (Lowe 2004) and the affine-scale invariant feature transform ASIFT (Morel and Yu 2009), that are used to successfully locate repeatable informative (invariant) features in images.

Matching surfaces while accounting for deformations was performed with conformal mappings (Lipman and Funkhouser 2009), embedding to finite dimensional Euclidean spaces (Elad and Kimmel 2001) and infinite ones (Bérard et al. 1994; Rustamov 2007), topological graphs (Hamza and Krim 2006; Wang et al. 2008), and exploiting the Gromov–Hausdorff distance (Mémoli and Sapiro 2005; Bronstein et al. 2006; Chazal et al. 2009). Which is just a subset of the numerous methods used in this exploding field. Another example, relevant to this paper is diffusion geometry, introduced in Coifman et al. (2005) for manifold learning that was first applied for shape analysis in Bronstein et al. (2010a). This geometry can be constructed from the eigen-structure of the Laplace–Beltrami operator. The same decomposition was recently used in Sun et al. (2009), Ovsjanikov et al. (2009), Ovsjanikov et al. (2010), Bronstein et al. (2010a) to

Communicated by C. Schnörr.

D. Raviv (✉)
Media Lab., MIT, Cambridge, MA, USA
e-mail: darav@mit.edu

R. Kimmel
Department of Computer Science, Technion, Haifa, Israel
e-mail: ron@cs.technion.ac.il

Published online: 14 June 2014

construct surface descriptors for shape retrieval and matching.

Some approaches in the field of shape matching, measure the discrepancy between surfaces and volumes by weighing the effort it takes to deform one geometric structure into another. Such geometric constructions can be used to define a Riemannian metric on the space of all possible shapes. These methods are popular, for example, in medical information analysis. They incorporate statistical priors (Davies et al. 2002), use spherical harmonics (Huang et al. 2005), exploit global symmetric deformations (Reuter et al. 2010), and use smooth diffeomorphic mappings (Beg et al. 2005). Statistics of curved domains can be utilized, for example, to overcome uncertainty, to evaluate different hypothesis, and compare between observations (Fletcher et al. 2003; Pennec 2006). The pseudo-metric proposed in this paper applies to the way a single shape is treated as a Riemannian structure rather than the space of all possible shapes as a whole.

In this paper, following the adoption of metric/differential geometry tools to image-analysis, we introduce a new geometry for affine invariant surface analysis. In Raviv et al. (2011a,b), the equi-affine invariant metric was first introduced to the surface analysis arena. Invariant curvatures were studied in Rugis and Klette (2006), Andrade and Lewiner (2012), and a scale invariant metric was the main theme of Aflalo et al. (2013), Bronstein and Kokkinos (2010). Here, we introduce a framework that handles affine transformations in its most general form including similarity. The proposed full affine invariant geometry for non-rigid surfaces copes with linear (affine) transformations including scaling and isometry.

The paper is organized as follows: In Sect. 2 we introduce the affine invariant pseudo-metric. Section 3 proves the invariance of the construction. In Sect. 4 numerical implementation considerations are discussed. Next, Sect. 5 briefly reviews some ideas behind diffusion geometry that could be used as a numerically stabilizing mechanism for the proposed geometry. Section 6 is dedicated to experimental results, and Sect. 7 concludes the paper.

2 Affine Metric Construction

We model a surface $(\mathcal{S}, g)$ as a compact two dimensional Riemannian manifold $\mathcal{S}$ with a metric tensor g. Let us further assume that $\mathcal{S}$ is embedded in $\mathbb{R}^3$ by a regular map $S : U \subset \mathbb{R}^2 \to \mathbb{R}^3$. The Euclidean metric tensor can be obtained from the re-parameterization invariant arc-length s of a parametrized curve $C(s)$ on $\mathcal{S}$. As the simplest Euclidean invariant is length, we search for the parameterization s that would satisfy $|C_s| = 1$, or explicitly,

$$
\begin{aligned}
1 &= \langle C_s, C_s \rangle = \langle S_s, S_s \rangle \\
&= \left\langle \frac{\partial S}{\partial u}\frac{du}{ds} + \frac{\partial S}{\partial v}\frac{dv}{ds}, \frac{\partial S}{\partial u}\frac{du}{ds} + \frac{\partial S}{\partial v}\frac{dv}{ds} \right\rangle \\
&= ds^{-2}\left(g_{11}du^2 + 2g_{12}dudv + g_{22}dv^2\right), \qquad (1)
\end{aligned}
$$

where

$$
g_{ij} = \langle S_i, S_j \rangle, \qquad (2)
$$

using the short hand notation $S_1 = \partial S/\partial u$, $S_2 = \partial S/\partial v$, where u and v are the coordinates of U. An infinitesimal displacement ds on the surface is thereby given by

$$
ds^2 = g_{11}du^2 + 2g_{12}dudv + g_{22}dv^2. \qquad (3)
$$

The metric coefficients $\{g_{ij}\}$ translate the surface parametrization coordinates u and v into a Euclidean invariant distance measure on the surface. This distance would not change under Euclidean transformations of the surface $RS+\mathbf{b}$ where R is a rotation matrix in $\mathbb{R}^3$. It would also be preserved w.r.t. isometric (length preserving) transformations.

The equi-affine transformation, defined by the linear operator $AS+\mathbf{b}$, where $\det(A) = 1$, requires a different treatment, see Blaschke (1923), Su (1983). Consider the curve $C \in \mathcal{S}$, parametrized by w. The equi-affine transformation is volume preserving, and thus, its invariant metric is constructed by restricting the volume defined by S_u, S_v, and C_{ww} to one. That is,

$$
\begin{aligned}
1 &= \det(S_u, S_v, C_{ww}) \\
&= \det\left(S_u, S_v, S_{ww}\right) \\
&= \det\left(S_u, S_v, S_{uu}\frac{du^2}{dw^2} + 2S_{uv}\frac{du}{dw}\frac{dv}{dw}\right. \\
&\qquad \left. + S_{vv}\frac{dv^2}{dw^2} + S_u\frac{d^2u}{dw^2} + S_v\frac{d^2v}{dw^2}\right) \\
&= dw^{-2}\det\left(S_u, S_v, S_{uu}du^2 + 2S_{uv}dudv + S_{vv}dv^2\right) \\
&= dw^{-2}\left(r_{11}du^2 + 2r_{12}dudv + r_{22}dv^2\right), \qquad (4)
\end{aligned}
$$

where now, the metric elements are given by

$$
r_{ij} = \det\left(S_1, S_2, S_{ij}\right), \qquad (5)
$$

and we extended the short hand notation to second order derivatives by which $S_{11} = \frac{\partial^2 S}{\partial u^2}$, $S_{22} = \frac{\partial^2 S}{\partial v^2}$, and $S_{12} = \frac{\partial^2 S}{\partial u \partial v}$. Note, that the second fundamental form in the Euclidean case is given by $b_{ij} = \sqrt{g}r_{ij}$ where $g = \det(g_{ij}) = g_{11}g_{22} - g_{12}^2$. The equi-affine re-parametrization invariant metric (Su 1983; Blaschke 1923) reads

$$
q_{ij} = |r|^{-\frac{1}{4}}r_{ij}, \qquad (6)
$$

where $r = \det(r_{ij}) = r_{11}r_{22} - r_{12}^2$.

This equi-affine metric applies to surfaces with positive Euclidean Gaussian curvature, that are oriented so as to provide positive squared distances. See also Raviv et al. (2011a). At hyperbolic points, when the Euclidean Gaussian curvature

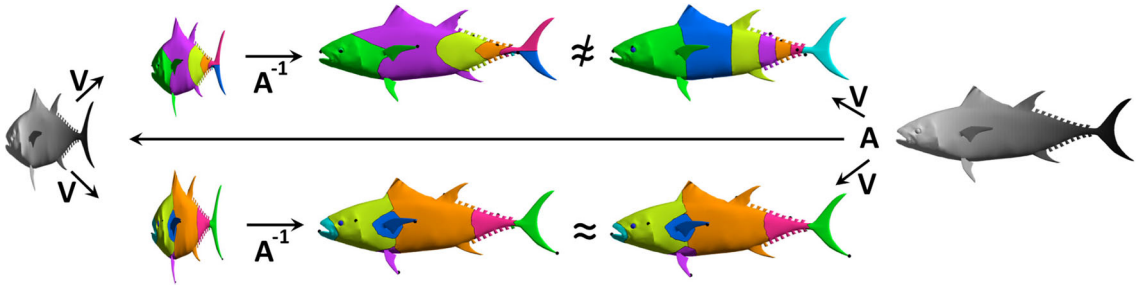

Fig. 1 Voronoi diagrams of ten points selected by farthest point sampling. Diffusion distances were used based on Euclidean metric (*top*) and an affine invariant one (*bottom*)

is negative, we have one positive and one negative eigenvalue of the metric r. In this case, we set the metric tensor to be zero. Numerically, we assign $(q_{ij}) = \epsilon\mathcal{I} = \epsilon \begin{pmatrix} 1 & 0 \\ 0 & 1 \end{pmatrix}$ metric to that point, where ϵ is a small constant. That is, such regions would practically be ignored by the proposed geometry (Raviv et al. 2013). Note that as S is a compact manifold, we can define a continuous shrinkage of the metric while the error is kept at the order of ϵ. In our implementation we chose a small ϵ at all hyperbolic and parabolic points. It was numerically validated and supported by the experimental results for the non-trivial surfaces reported in this paper.

Next, we resort to the similarity (scale and isometry) invariant metric proposed in Aflalo et al. (2013). Scale invariance is obtained by multiplying the metric by the Gaussian curvature. In metric notations, the Gaussian curvature K is defined as the ratio between the determinants of the second and the first fundamental forms. We propose to compute the Gaussian curvature with respect to the equi-affine invariant metric, and then construct a new metric by multiplying the equi-affine metric elements by the equi-affine Gaussian curvature. Specifically, consider the surface $(\mathcal{S}, q)$, where q_{ij} is the equi-affine invariant pseudo-metric, and compute the equi-affine Gaussian curvature K^q of $(\mathcal{S}, q)$ at each point. The affine invariant pseudo-metric is then defined by

$$h_{ij} = \left|K^q\right| q_{ij}. \tag{7}$$

Let us next prove the affine invariance of the above construction for surfaces.

3 Invariance Properties

In this section we prove affine invariance of the proposed pseudo-metric. Let us first justify the scale invariant metric constructed by multiplication of a given Euclidean metric by the Gaussian curvature.

Theorem 1 *Let K be the Gaussian curvature of a surface S, and g_{ij} the elements of its Riemannian metric. Then, $|K|g_{ij}$ is a scale invariant metric.*

Proof Let the surface S be scaled by a scalar $\alpha > 0$, such that

$$\tilde{S}(u, v) = \alpha S(u, v). \tag{8}$$

In what follows, we omit the surface parameterization u, v for brevity, and denote the a quantity y computed for the scaled surface by $\tilde{y}$. The first and second fundamental forms are scaled by α^2 and α respectively,

$$\begin{aligned} \tilde{g}_{ij} &= \langle \alpha S_i, \alpha S_j \rangle = \alpha^2 \langle S_i, S_j \rangle = \alpha^2 g_{ij}, \\ \tilde{b}_{ij} &= \langle \alpha S_{ij}, N \rangle = \alpha \langle S_{ij}, N \rangle = \alpha b_{ij}, \end{aligned} \tag{9}$$

which yields

$$\begin{aligned} \det(\tilde{g}) &= \alpha^4 \det(g) \\ \det(\tilde{b}) &= \alpha^2 \det(b). \end{aligned} \tag{10}$$

Since the Gaussian curvature is the ratio between the determinants of the second and first fundamental forms, we readily have that

$$\tilde{K} \equiv \frac{\det(\tilde{b})}{\det(\tilde{g})} = \frac{\alpha^2 \det(b)}{\alpha^4 \det(g)} = \frac{1}{\alpha^2} K, \tag{11}$$

from which we conclude that multiplying the Euclidean metric by the magnitude of its Gaussian curvature indeed provides a scale invariant metric. That is,

$$|\tilde{K}|\tilde{g}_{ij} = \left|\frac{1}{\alpha^2} K\right| \alpha^2 g_{ij} = |K| g_{ij}. \tag{12}$$

□

Theorem 2 *Let $r_{ij} = \det\left(S_1, S_2, S_{ij}\right)$, and $q_{ij} = |r|^{-\frac{1}{4}} r_{ij}$, then, q_{ij} is an equi-affine invariant quadratic form.*

For proof see Su (1983).

Corollary 1 *Let $Q = (q_{ij}) = \mathbf{U}\Gamma\mathbf{U}^{\mathrm{T}}$ and $\Gamma = \begin{pmatrix} \gamma_1 & 0 \\ 0 & \gamma_2 \end{pmatrix}$ then,*

$$\hat{Q} = \begin{cases} \mathbf{U} \begin{pmatrix} |\gamma_1| & 0 \\ 0 & |\gamma_2| \end{pmatrix} \mathbf{U}^{\mathrm{T}} & \text{if } sign(\gamma_1) sign(\gamma_2) > 0 \\ 0 & \text{if } sign(\gamma_1) sign(\gamma_2) \leq 0, \end{cases}$$

is an equi-affine invariant pseudo-metric.

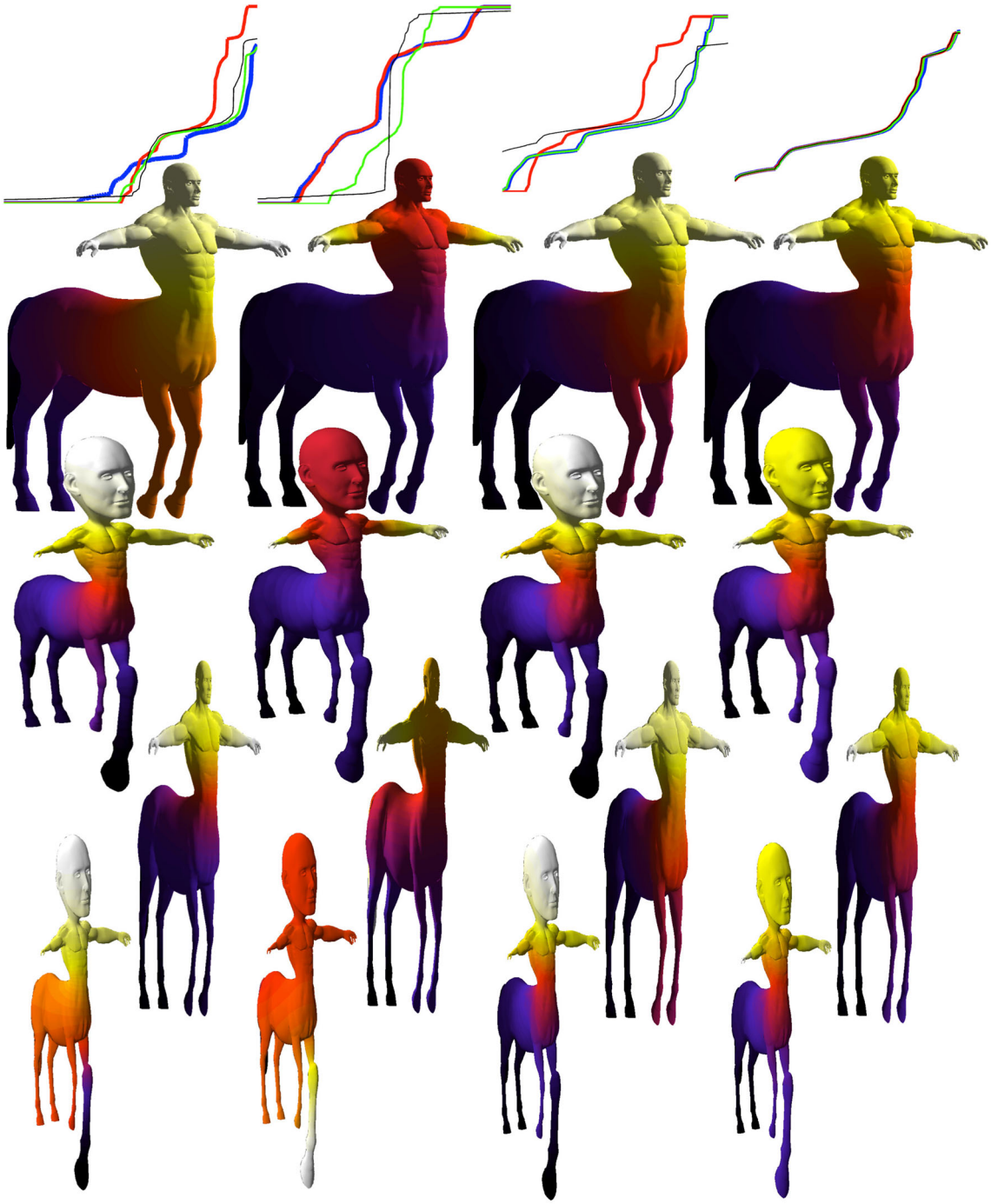

Fig. 2 The 9'th LBO eigenfunction textured mapped on the surface using four different metrics, from *left* to *right*: Euclidean, scale-invariant, equi-affine, and affine. Deformations from *top* to *bottom*: None, local scale, equi-affine, and affine. At the top, the accumulated (*histogram*) values of the eigenfunction are displayed. The *blue curve* depicts the original shape, *red* the a locally scaled one, *green* the equi-affine and *black* the affine transformation (Color figure online)

Proof According to Su (1983), the tensor Q is re-parametriza tion equi-affine invariant form for all elliptic points. For all elliptic points with $\gamma_1, \gamma_2 > 0$, we have the local metric structure $\hat{Q} = Q$. For all elliptic points with $\gamma_1, \gamma_2 <$ 0, we use our freedom of surface orientation to obtain positive distances. In other words, by virtually changing the surface orientation we obtain a re-parametrization invariant metric structure with two positive eigenvalues,

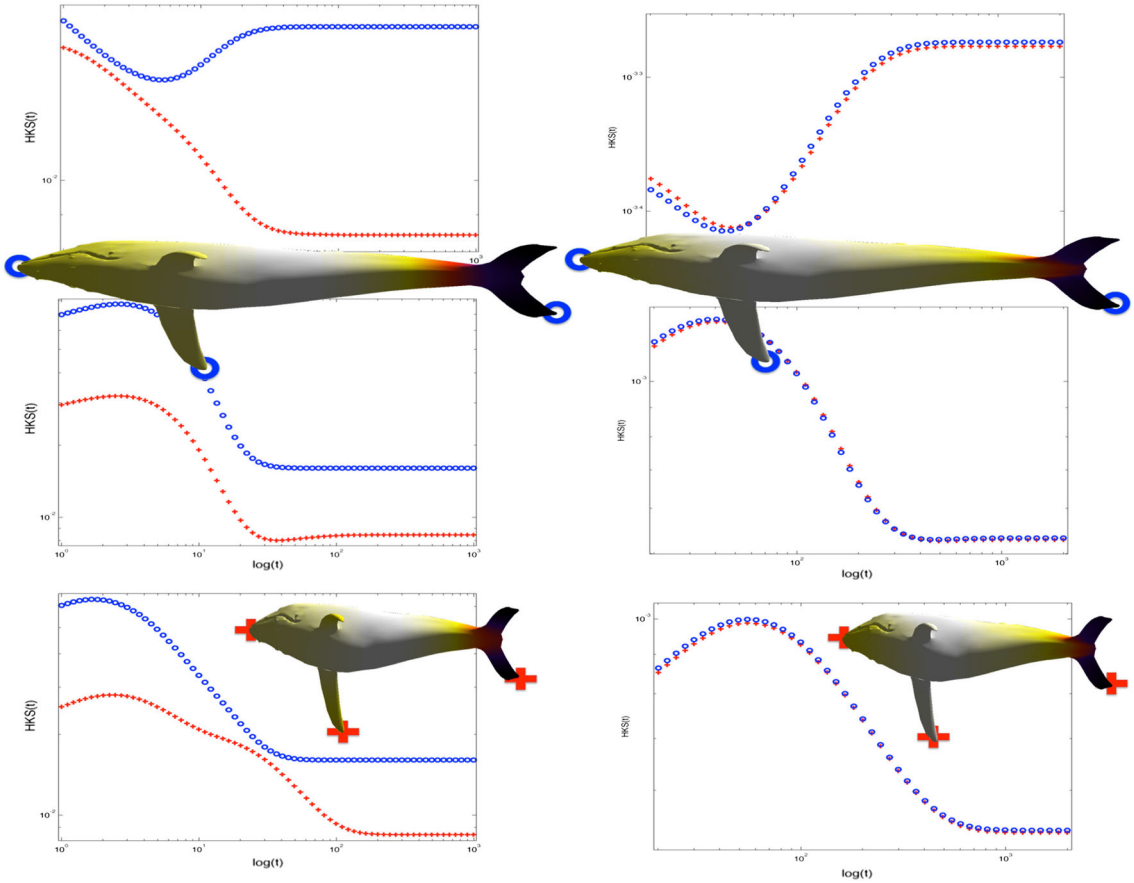

Fig. 3 Affine heat kernel signatures for the regular metric (*left*), and the invariant version (*right*). The *blue circles* represent the signatures for three points on the original surface, while the *red plus signs* are computed for the deformed version. Using log–log axes, we plot the scaled-HKS as a function of t (Color figure online)

$\hat{Q} = \mathbf{U}\begin{pmatrix} |\gamma_1| & 0 \\ 0 & |\gamma_2| \end{pmatrix}\mathbf{U}^{\mathrm{T}}$. For all hyperbolic, and parabolic points we have a trivial invariant $\hat{Q} = 0$, that altogether construct the equi-affine invariant pseudo-metric. □

Using Brioschi formula (Gray et al. 2006) we can evaluate the Gaussian curvature directly from the metric and its first and second derivatives. Specifically, given the metric tensor q_{ij}, we have

$$K^q \equiv \frac{\beta - \gamma}{\det^2(q)}, \tag{13}$$

where

$$\beta = \det\begin{pmatrix} -\frac{1}{2}q_{11,vv} + q_{12,vu} - \frac{1}{2}q_{22,uu} & \frac{1}{2}q_{11,u} & q_{12,u} - \frac{1}{2}q_{11,v} \\ q_{12,v} - \frac{1}{2}q_{22,u} & q_{11} & q_{12} \\ \frac{1}{2}q_{22,v} & q_{12} & q_{22} \end{pmatrix}$$

$$\gamma = \det\begin{pmatrix} 0 & \frac{1}{2}q_{11,v} & \frac{1}{2}q_{22,u} \\ \frac{1}{2}q_{11,v} & q_{11} & q_{12} \\ \frac{1}{2}q_{22,u} & q_{12} & q_{22} \end{pmatrix}, \tag{14}$$

here $q_{ij,u}$ denotes the derivation of q_{ij} with respect to u, and in a similar manner $q_{ij,uv}$ is the second derivative w.r.t. u and v. Same notations follow for $q_{ij,v}$, $q_{ij,vv}$, and $q_{ij,uu}$.

Corollary 2 *Let q be the equi-affine metric. Then, K^q is an equi-affine invariant curvature.*

Proof From Brioschi's formula we have that the curvature can be evaluated directly from the metric and its derivatives. Hence, as by Corollary 1 the metric is equi-affine invariant, it follows that so does the equi-affine Gaussian curvature. □

Corollary 3 *Let K^q be the equi-affine invariant Gaussian curvature, then the metric defined by $h_{ij} = |K^q|\, q_{ij}$ is scale invariant.*

Proof Scaling the surface S by α, the corresponding equi-affine invariant components are

$$\begin{aligned} \tilde{r}_{ij} &= \det(\alpha S_1, \alpha S_2, \alpha S_{ij}) = \alpha^3 r_{ij} \\ \tilde{r}_{ij,u} &= \alpha^3 r_{ij,u} \\ \tilde{r}_{ij,uv} &= \alpha^3 r_{ij,uv} \\ \det(\tilde{r}) &= \alpha^6 \det(r), \end{aligned} \tag{15}$$

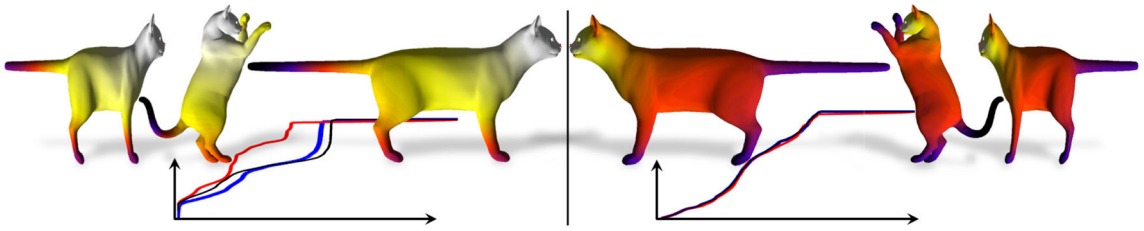

Fig. 4 Diffusion distances—Euclidean (*left*) and affine (*right*)—is measured from the nose of the cat after non-uniform scaling and stretching. The accumulated (*histogram*) distances (*at the bottom*) are color-coded as in Fig. 2 (Color figure online)

that leads to

$$\tilde{q}_{ij} = \frac{\tilde{r}_{ij}}{(\det(\tilde{r}))^{\frac{1}{4}}} = \frac{\alpha^3 r_{ij}}{(\alpha^6 \det(r))^{\frac{1}{4}}} = \alpha^{\frac{3}{2}} q_{ij}, \tag{16}$$

that yields $\det(\tilde{q}) = \left(\alpha^{\frac{3}{2}}\right)^2 \det(q) = \alpha^3 \det(q)$. Denote the equi-affine Gaussian curvature of the scaled surface $\tilde{S} = \alpha S$ by $\tilde{K}^q$. We have that

$$\tilde{\beta} = \left(\alpha^{\frac{3}{2}}\right)^3 \beta,$$

$$\tilde{\gamma} = \left(\alpha^{\frac{3}{2}}\right)^3 \gamma,$$

$$\tilde{K}^q = \frac{\tilde{\beta} - \tilde{\gamma}}{\det^2(\tilde{q})} = \frac{\left(\alpha^{\frac{3}{2}}\right)^3 (\beta - \gamma)}{\left(\alpha^3\right)^2 \det^2(q)} = \alpha^{-\frac{3}{2}} K^q. \tag{17}$$

It immediately follows that

$$|\tilde{K}^q| \tilde{q}_{ij} = |\tilde{K}^q| \alpha^{\frac{3}{2}} q_{ij} = |\alpha^{-\frac{3}{2}} K^q| \alpha^{\frac{3}{2}} q_{ij} = |K^q| q_{ij} \tag{18}$$

which concludes the proof. □

Theorem 3 *h_{ij} is an affine invariant pseudo-metric.*

Proof Putting corollaries 1, 2 and 3 together, we obtain the main result of this paper; Namely, h_{ij} is equi-affine invariant as well as scale invariant and thus affine invariant. □

4 Implementation Considerations

Given a triangulated surface we use the Gaussian curvature approximation proposed in Meyer et al. (2003) while operating on the equi-affine metric tensor. The Gaussian curvature for smooth surfaces can be defined using the Global Gauss-Bonnet Theorem, see Do Carmo (1976). Polthier and Schmies used this property to approximate the Gaussian curvature of triangulated surfaces in Polthier and Schmies (1998). Given a vertex in a triangulated mesh that is shared by p triangles such that the angle of each triangle at that vertex is given by θ_i, where $i \in 1, \ldots, p$. The Gaussian curvature K at that vertex can be approximated by

$$K \cong \frac{1}{\frac{1}{3}\sum_{i=1}^{p} \mathcal{A}_i} \left(2\pi - \sum_{i=1}^{p} \theta_i\right), \tag{19}$$

where $\mathcal{A}_i$ is the area of the i-th triangle, and θ_i is the corresponding angle of the i-th triangle touching the vertex for which K is being approximated.

The metric tensor translates angles, distances, and areas from the parametric plane to the surface. Let us justify some known relations, as we use them in our numerical construction of the affine metric.

Corollary 4 *Consider a triangle $ABC = \{S(u_0, v_0), S(u_0 + du, v_0), S(u_0, v_0 + dv)\}$, infinitesimally defined on the surface $S(u, v)$ with metric (q_{ij}), then,*

$$\cos\theta_A = \frac{q_{12}}{\sqrt{q_{11} q_{22}}}. \tag{20}$$

Proof Consider the above infinitesimal triangle ABC. For simplicity of notations let $du = dv = 1$. The length of the edges of the triangle would then be $l_c^2 = (1\,0)(q_{ij})(1\,0)^T = q_{11}$, $l_b^2 = q_{22}$, and $l_a^2 = (1\,1)(q_{ij})(1\,1)^T = q_{11} - 2q_{12} + q_{22}$. From the law of cosines we readily have that

$$\cos\theta_A = \frac{q_{11} + q_{22} - (q_{11} - 2q_{12} + q_{22})}{2\sqrt{q_{11} q_{22}}} = \frac{q_{12}}{\sqrt{q_{11} q_{22}}}.$$

□

Corollary 5 *The area of the above triangle can be expressed by the metric coefficients as $\mathcal{A}_{ABC} = \frac{1}{2}\sqrt{\det(q_{ij})}$.*

Proof From Corollary 4 we have that

$$\sin^2\theta_A = 1 - \left(\frac{q_{12}}{\sqrt{q_{11} q_{22}}}\right)^2 = \frac{q_{11} q_{22} - q_{12}^2}{q_{11} q_{22}}.$$

The area of the triangle is half the length of its base multiplied by its height,

$$\mathcal{A}_{ABC} = \frac{1}{2}\sqrt{q_{22}} \left(\sqrt{q_{11}} \sqrt{\frac{q_{11} q_{22} - q_{12}^2}{q_{11} q_{22}}}\right) = \frac{1}{2}\sqrt{\det(q_{ij})}.$$

□

Consider the surface S given by its three coordinate functions $x(u, v)$, $y(u, v)$ and $z(u, v)$, where, for example, $x : U \in \mathbb{R}^2 \to \mathbb{R}$, and

$$S(u, v) = \begin{pmatrix} x(u, v) \\ y(u, v) \\ z(u, v) \end{pmatrix}. \tag{21}$$

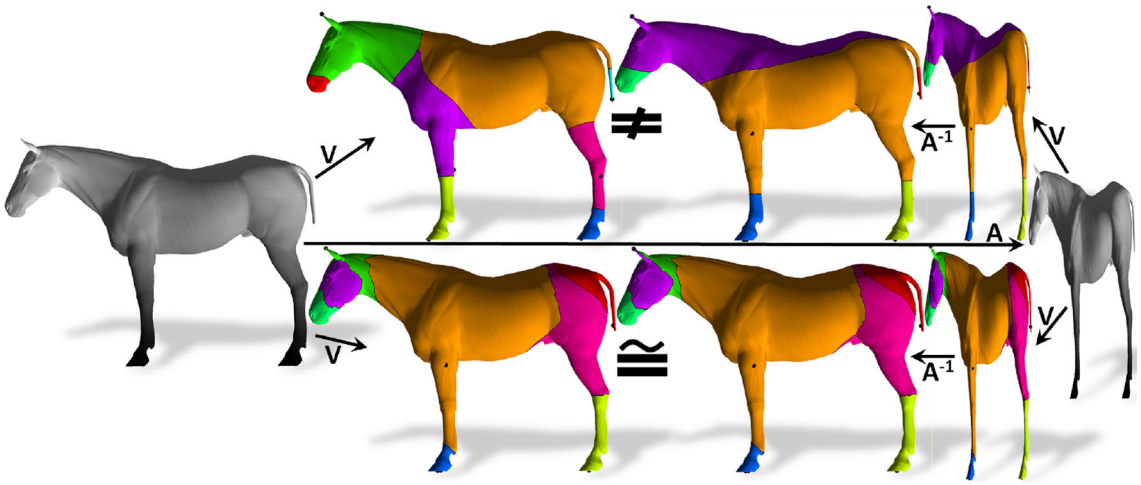

Fig. 5 Voronoi diagrams using ten points selected by the farthest point sampling strategy. The commute time distances were evaluated using the Euclidean metric (*top*) and the proposed affine one (*bottom*)

In order to evaluate the equi-affine metric the surface is first locally approximated by a quadratic form. For each triangle we approximate

$$S(u,v) = \begin{pmatrix} x(u,v) \\ y(u,v) \\ z(u,v) \end{pmatrix} \approx C \begin{pmatrix} 1 \\ u \\ v \\ uv \\ u^2 \\ v^2 \end{pmatrix}. \tag{22}$$

where the matrix $C_{3\times 6}$ contains 18 parameters. The local coefficients matrix C is evaluated from six surface points (vertices). Three vertices belong to the triangle for which the metric is evaluated, and three to its nearest neighboring triangles.

The equi-affine metric coefficients for each triangle are then evaluated from our local quadratic approximation of $S(u,v)$ and its corresponding derivatives. Finally, the Gaussian curvature with respect to the equi-affine metric is approximated for each vertex from the local area and angle distortions as defined by the metric, see Eq. (19). In order to construct the full-affine invariant metric we need to scale the equi-affine metric by the equi-affine Gaussian curvature. To that end, the curvature is linearly interpolated, from its values at the vertices, at the center of each triangle.

Finally, following Raviv et al. (2011a), we use the finite elements method (FEM) presented in Dziuk (1988) to compute the spectral decomposition of the affine invariant Laplace–Beltrami operator constructed from the metric provided by Eq. (7). The decomposition based on an affine invariant pseudo-metric provides invariant eigenvectors and corresponding invariant eigenvalues.

The equi-affine metric is well defined only at elliptic points (Su 1983), that is, points with positive Euclidean Gaussian curvature. At parabolic and hyperbolic points the equi-affine metric trivially degenerates to zero, while at elliptic points the local surface orientation is defined so as to provide positive distances. In order, to numerically handle non-elliptic surface points we assigned a small $\epsilon\mathcal{I}$ to be the metric matrix. The $O(\epsilon)$ error introduced to geodesic distances measured with such a regularization is bounded by $\epsilon\mathcal{D}$, where $\mathcal{D}$ is the diameter of the surface. As many interesting shapes are dominated by elliptic points, the error is often smaller than the above upper bound.

5 Metric Invariant Diffusion Geometry

Diffusion Geometry introduced in Coifman et al. (2005); Coifman and Lafon (2006), deals with geometric analysis of metric spaces where usual distances are replaced by integral difference between heat kernels. The *heat equation*

$$\left(\frac{\partial}{\partial t} + \Delta_h\right) f(x,t) = 0, \tag{23}$$

describes the propagation of heat, where $f(x,t)$ is the heat distribution at a point x in time t. Initial conditions are given as $f(x,0)$, and Δ_h is the Laplace Beltrami operator with respect to the metric h. The fundamental solution of (23) is called a *heat kernel*, and using spectral decomposition it can be written as

$$k_t(x,x') = \sum_{i\geq 0} e^{-\lambda_i t}\phi_i(x)\phi_i(x'), \tag{24}$$

where ϕ_i and λ_i are the corresponding eigenfunctions and eigenvalues of the Laplace–Beltrami operator satisfying

$$\Delta_h\phi_i = \lambda_i\phi_i. \tag{25}$$

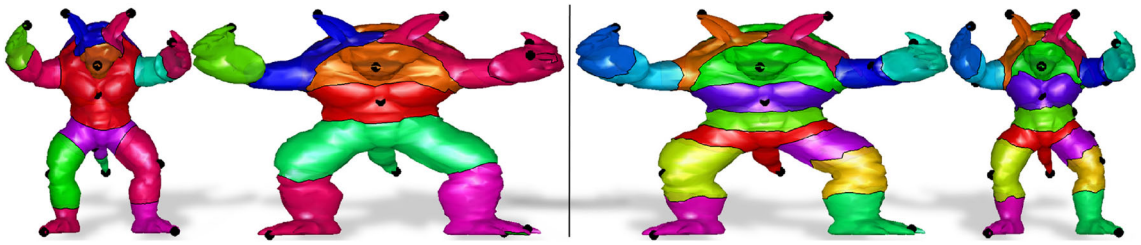

Fig. 6 Matching two shapes using the GMDS Bronstein et al. (2006) framework with diffusion distances. The affine (*right*) metric finds the proper correspondence as expected unlike the Euclidean one (*left*) which is sensitive to non-uniform stretching. Corresponding surface segments share the *same color* (Color figure online)

As the Laplace–Beltrami operator is an *intrinsic* geometric quantity, it can be expressed in terms of a metric h of the surface $\mathcal{S}$.

The value of the heat kernel $k_t(x, x')$ can be interpreted as the transition probability density of a random walk of length t from point x to point x'. The length for time t defines a family of diffusion distances

$$d_t^2(x, x') = \int \left(k_t(x, \cdot) - k_t(x', \cdot)\right)^2 da = \sum_{i>0} e^{-2\lambda_i t}(\phi_i(x) - \phi_i(x'))^2, \quad (26)$$

between any two surface points x and x'. Special attention was given to the diagonal of the kernel $k_t(x, x)$, that was proposed as robust local descriptor, and referred to as the *heat kernel signatures* (HKS), by Sun et al. in Sun et al. (2009).

6 Experimental Results

The first experiment presents eigenfunctions of the Laplace Beltrami operator defined by various metrics and different deformations. In Fig. 2 we present the 9'th eigenfunction textured mapped on the surface using a Euclidean metric, scale invariant, equi-affine and the proposed affine invariant pseudo-metric. At each row a different deformation of the surface is presented. Local scaling was applied to the shapes at the second row, while surfaces on the third row underwent volume preserving stretching (equi-affine). The bottom row shows a full affine transformation that was applied to the surface (including local scaling). The accumulated histogram values of the corresponding 9'th eigenfunction are plotted at the top of each column. Blue is used for the original shape, red for the locally scaled one, green for the equi-affine transformed one, and black for the affine transformed version.

In the second experiment, shown in Fig. 3, we evaluate the Heat Kernel Signatures of a surface subject to an affine transformation using the Euclidean metric and the affine pseudo-metric. We plot the signatures using log-log axes for three different corresponding points on the surfaces.

The third experiment, Fig. 4 shows diffusion distances measured from the nose of a cat after anisotropic scaling and stretching as well as an almost isomeric pose transformation.

Next, we compute the Voronoi diagrams for ten points selected by the farthest point sampling strategy, as seen in Figs. 1 and 5. Distances are measured with the global scale invariant commute time distances (Qiu and Hancock 2007), and diffusion distances receptively, using a Euclidean and the proposed affine metrics. Again, the affine metric is proven to be invariant to affine transformations as expected.

In the next experiment we used the affine metric for finding the correspondence between two shapes. We used the GMDS framework (Bronstein et al. 2006) with diffusion distances using the same initialization for both experiments. Figure 6 displays the Voronoi cells of matching surface segments.

Finally, we evaluated the proposed metric on the SHREC 2010 dataset (Bronstein et al. 2010b) using the shapeGoogle framework (Ovsjanikov et al. 2009), while introducing four new deformations; equi-affine, isometry and equi-affine, affine, and a combination of isometry and affine. Table 1 shows that the new affine metric discriminative power is as good as the Euclidean one, performs well on scaling as the scale invariant metric, and similar to the equi-affine one for handling volume preserving affine transformations. Moreover, the new metric is the only one capable of dealing with the full affine deformations. Note that shapes which were considered to be locally scaled in that database, were in fact treated with an offset operation (morphological erosion) rather than scaling. This explains part of the performance degradation in the local scale examples.

Performance was evaluated using precision/recall characteristics. *Precision* $\mathrm{P}(r)$ is defined as the percentage of relevant shapes in the first r top-ranked retrieved shapes. *Mean average precision* (mAP) is defined as $\mathrm{mAP} = \sum_r \mathrm{P}(r) \cdot \mathrm{rel}(r)$, where $\mathrm{rel}(r)$ the relevance of a given rank, was used as a single measure of performance. Intuitively, mAP is interpreted as the area below the precision-recall curve.

Table 1 Performance of different metrics with shape Google framework (mAP in %)

Transformation	Strength 1	≤2	≤3	≤4	≤5
Affine invariant pseudo-metric					
Isometry	100.00	100.00	100.00	100.00	100.00
Micro holes	100.00	100.00	100.00	100.00	100.00
Noise	100.00	100.00	100.00	98.72	98.97
Shot noise	100.00	100.00	98.72	97.60	97.05
Scale	28.87	56.74	61.42	53.75	47.77
Local scale	100.00	100.00	98.72	91.79	87.40
Equi-affine	100.00	98.08	92.52	87.72	83.05
Iso + equi-affine	100.00	97.12	92.95	85.32	79.99
Affine	88.46	77.79	70.81	65.21	61.21
Isometry + affine	88.46	77.82	73.76	68.35	64.60
Scale invariant metric					
Isometry	100.00	100.00	100.00	100.00	100.00
Micro holes	100.00	92.12	84.66	78.90	74.96
Noise	100.00	95.00	92.42	87.49	81.62
Shot noise	100.00	100.00	97.01	94.94	92.21
Scale	100.00	100.00	100.00	100.00	100.00
Local scale	100.00	97.44	94.87	90.21	82.98
Equi-affine	81.03	72.35	65.82	61.55	59.86
Iso + equi-affine	81.03	74.13	63.93	61.17	62.30
Affine	100.00	90.87	87.36	84.64	81.99
Isometry + affine	100.00	93.75	89.64	84.33	83.11
Equi-affine invariant pseudo-metric					
Isometry	100.00	100.00	100.00	100.00	100.00
Micro holes	100.00	100.00	100.00	100.00	100.00
Noise	100.00	100.00	91.88	83.72	75.62
Shot noise	100.00	100.00	100.00	97.12	92.31
Scale	29.82	50.81	48.34	43.16	39.89
Local scale	100.00	100.00	95.51	87.81	81.08
Equi-affine	100.00	100.00	100.00	100.00	100.00
Iso + equi-affine	100.00	100.00	100.00	100.00	100.00
Affine	75.90	60.35	52.54	47.82	43.86
Isometry + affine	75.46	59.59	52.08	47.39	44.34
Affine invariant pseudo-metric					
Isometry	100.00	100.00	98.72	99.04	99.23
Micro holes	100.00	100.00	98.08	97.02	95.53
Noise	100.00	95.51	94.02	94.55	94.87
Shot noise	100.00	100.00	100.00	99.04	97.69
Scale	94.87	97.44	98.29	95.03	92.40
Local scale	100.00	100.00	98.29	96.47	92.07
Equi-affine	100.00	100.00	96.79	96.63	96.08
Iso + equi-affine	100.00	98.08	93.80	94.39	94.36
Affine	96.15	95.51	95.73	95.83	96.67
Isometry+affine	96.15	98.08	97.44	98.08	98.46

Ideal retrieval (mAP=100 %) is achieved when all queries provide the correct answer as first match. Performance results are summarized by the transformation class and strength.

7 Conclusions

A new affine invariant pseudo-metric for surfaces was introduced. Assuming the limbs of an articulated objects are connected with non-elliptic regions, the proposed differential structure allows us to cope with per-limb stretching and scaling of the surface. We demonstrated the proposed geometry by incorporating it with known shape analysis tools that were evaluated by computing the correspondence, matching, and retrieval of synthetic surfaces. The power to deal with a richer set of transformations when analyzing shapes has already proven to be useful in the analysis of textured shapes as shown in Kovnatsky et al. (2012). We hope that the proposed affine geometry could be found useful in the future for shape processing and analysis applicants.

Acknowledgments We thank the editor and the reviewers for their valuable comments that helped us improve the presentation and writeup of the paper. This research was supported by the Office of Naval Research (ONR) award number N00014-12-1-0517 and by Israel Science Foundation (ISF) Grant Number 1031/12.

References

Aflalo, Y., Kimmel, R., & Raviv, D. (2013). Scale invariant geometry for nonrigid shapes. *SIAM Journal on Imaging Sciences*, *6*(3), 1579–1597.

Alvarez, L., Guichard, F., Lions, P.-L., & Morel, J.-M. (1993). Axioms and fundamental equations of image processing. *Archive for Rational Mechanics and Analysis*, *123*(3), 199–257.

Andrade, M., & Lewiner, T. (2012). Affine-invariant curvature estimators for implicit surfaces. *Computer Aided Geometric Design*, *29*(2), 162–173.

Beg, M. F., & Miller, M. I. (2005). Computing large deformation metric mappings via geodesic flows of diffeomorphisms. *International Journal of Computer Vision (IJCV)*, *61*(2), 139–157.

Bérard, P., Besson, G., & Gallot, S. (1994). Embedding Riemannian manifolds by their heat kernel. *Geometric and Functional Analysis*, *4*(4), 373–398.

Blaschke, W. (1923). *Vorlesungen uber Differentialgeometrie und geometrische Grundlagen von Einsteins Relativitatstheorie, vol. 2*. Berlin: Springer.

Bronstein, M. M., & Kokkinos, I. (2010). Scale-invariant heat kernel signatures for non-rigid shape recognition. In *Proceedings of Computer Vision and Pattern Recognition (CVPR)*.

Bronstein, A. M., Bronstein, M. M., & Kimmel, R. (2006). Efficient computation of isometry-invariant distances between surfaces. *SIAM Journal on Scientific Computing*, *28*(5), 1812–1836.

Bronstein, A. M., Bronstein, M. M., Kimmel, R., Mahmoudi, M., & Sapiro, G. (2010a). A Gromov–Hausdorff framework with diffusion geometry for topologically-robust non-rigid shape matching. *International Journal of Computer Vision (IJCV)*, *89*(2–3), 266–286.

Bronstein, A. M., Bronstein, M. M., Castellani, U., Falcidieno, B., Fusiello, A., Godil, A., Guibas, L. J., Kokkinos, I., Lian, Z., Ovsjanikov, M., Patané, G., Spagnuolo, M., & Toldo, R. (2010b) . SHREC 2010: Robust large-scale shape retrieval benchmark. In *Proceedings of Workshop on 3D Object Retrieval (3DOR)*.

Brook, A., Bruckstein, A.M., & Kimmel, R. (2005). On similarity-invariant fairness measures. In *Scale-space, LNCS 3459* (pp. 456–467). Hofgeismar, Germany: Springer, 7–9 April 2005.

Bruckstein, A. M., & Netravali, A. N. (1995). On differential invariants of planar curves and recognizing partially occluded planar shapes. *Annals of Mathematics and Artificial Intelligence (AMAI)*, *13*(3–4), 227–250.

Bruckstein, A. M., & Shaked, D. (1998). Skew symmetry detection via invariant signatures. *Pattern Recognition*, *31*(2), 181–192.

Bruckstein, A. M., Rivlin, E., & Weiss, I. (1997). Scale-space local invariants. *Image and Vision Computing*, *15*(5), 335–344.

Bruckstein, A. M., Katzir, N., Lindenbaum, M., & Porat, M. (1992). Similarity-invariant signatures for partially occluded planar shapes. *International Journal of Computer Vision*, *7*(3), 271–285.

Bruckstein, A. M., Holt, R. J., Netravali, A. N., & Richardson, T. J. (1993). Invariant signatures for planar shape recognition under partial occlusion. *Computer Vision, Graphics, and Image Processing: Image Understanding*, *58*, 49–65.

Calabi, E., Olver, P. J., Shakiban, C., Tannenbaum, A., & Haker, S. (1998). Differential and numerically invariant signature curves applied to object recognition. *International Journal of Computer Vision*, *26*, 107–135.

Carlsson, S., Mohr, R., Moons, T., Morin, L., Rothwell, C. A., Van Diest, M., et al. (1996). Semi-local projective invariants for the recognition of smooth plane curves. *International Journal of Computer Vision*, *19*(3), 211–236.

Chazal, F., Cohen-Steiner, D., Guibas, L. J., Mémoli, F., & Oudot, S. (2009). Gromov–Hausdorff stable signatures for shapes using persistence. *Computer Graphics Forum*, *28*(5), 1393–1403.

Cohignac, T., Lopez, C., & Morel, J. M. (1994). Integral and local affine invariant parameter and application to shape recognition, vol. 1. In *Proceedings of the 12th IAPR International Conference on Pattern Recognition (ICPR)* (pp. 164–168), October 1994.

Coifman, R. R., & Lafon, S. (2006). Diffusion maps. *Applied and Computational Harmonic Analysis*, *21*, 5–30.

Coifman, R. R., Lafon, S., Lee, A. B., Maggioni, M., Nadler, B., Warner, F., et al. (2005). Geometric diffusions as a tool for harmonic analysis and structure definition of data: Diffusion maps. *PNAS*, *102*(21), 7426–7431.

Davies, R. H., Twining, C. J., Cootes, T. F., Waterton, J. C., & Taylor, C. J. (2002). A minimum description length approach to a minimum description length approach to statistical shape modeling. *IEEE Transactions on Medical Imaging*, *21*(5), 525–537.

Do Carmo, M. P. (1976). *Differential geometry of curves and surfaces*. Englewood Cliffs, NJ: Prentice-Hall.

Dziuk, G. (1988). Finite elements for the Beltrami operator on arbitrary surfaces. In *Partial differential equations and calculus of variations* (pp. 142–155).

Elad, A., & Kimmel, R. (2001). Bending invariant representations for surfaces. In *Proceedings of Computer Vision and Pattern Recognition (CVPR)* (pp. 168–174).

Fletcher, P. T., Joshi, S., Lu, C., & Pizer, S. (2003). Gaussian distributions on Lie groups and their application to statistical shape analysis. In *Proceedings of Information Processing in Medical Imaging (IPMI)* (pp. 450–462).

Gray, A., Abbena, E., & Salamon, S. (2006). *Modern differential geometry of curves and surfaces with mathematica* (3rd ed.). Boca Raton, FL: CRC Press.

Hamza, A. B., & Krim, H. (2006). Geodesic matching of triangulated surfaces. *IEEE Transactions on Image Processing*, *15*(8), 2249–2258.

Huang, H., Shen, L., Zhang, R., Makedon, F., Hettleman, B., & Pearlman, J. D. (2005). Surface alignment of 3D spherical harmonic models: Application to cardiac MRI analysis. In *Proceedings of Medical Image Computing and Computer Assisted Intervention (MICCAI)*.

Kimmel, R. (1996). Affine differential signatures for gray level images of planar shapes, vol. 1. In *IEEE Proceedings of the 13th International Conference on Pattern Recognition* (pp. 45–49). Vienna, Austria: IEEE, 25–30 August 1996.

Kovnatsky, A., Bronstein, M. M., Raviv, D., Bronstein, A. M., & Kimmel, R. (2012). Affine-invariant photometric heat kernel signatures. In *Proceedings of Eurographics workshop on 3D object retrieval (3DOR)*.

Ling, H., & Jacobs, D. W. (2005). Using the inner-distance for classification of articulated shapes, vol. 2. In *Proceedings of Computer Vision and Pattern Recognition (CVPR)* (pp. 719–726), San Diego, USA, 20–26 June 2005.

Lipman, Y., & Funkhouser, T. (2009). Möbius voting for surface correspondence, vol. 28. In *Proceedings of ACM Transactions on Graphics (SIGGRAPH)*.

Lowe, D. (2004). Distinctive image features from scale-invariant keypoint. *International Journal of Computer Vision (IJCV)*, *60*(2), 91–110.

Mémoli, F., & Sapiro, G. (2005). A theoretical and computational framework for isometry invariant recognition of point cloud data. *Foundations of Computational Mathematics*, *5*(3), 313–347.

Meyer, M., Desbrun, M., Schroder, P., & Barr, A. H. (2003). Discrete differential-geometry operators for triangulated 2-manifolds. *Visualization and Mathematics*, *III*, 35–57.

Moons, T., Pauwels, E., Van Gool, L. J., & Oosterlinck, A. (1995). Foundations of semi-differential invariants. *International Journal of Computer Vision (IJCV)*, *14*(1), 25–48.

Morel, J. M., & Yu, G. (2009). ASIFT: A new framework for fully affine invariant image comparison. *SIAM Journal on Imaging Sciences*, *2*, 438–469.

Olver, P. J. (1999). Joint invariant signatures. *Foundations of Computational Mathematics*, *1*, 3–67.

Olver, P. J. (2005). A survey of moving frames. In H. Li, P. J. Olver, & G. Sommer (Eds.), *Computer algebra and geometric algebra with applications* (pp. 105–138)., LNCS 3519 New York: Springer.

Ovsjanikov, M., Bronstein, A. M., Bronstein, M. M., & Guibas, L. J. (2009). Shape Google: A computer vision approach to invariant shape retrieval. In *Proceedings of Non-Rigid Shape Analysis and Deformable Image Alignment (NORDIA)*.

Ovsjanikov, M., Mérigot, Q., Mémoli, F., & Guibas, L. J. (2010). One point isometric matching with the heat kernel, vol. 29. In *Proceedings of Symposium on Geometry Processing (SGP)* (pp. 1555–1564).

Pauwels, E., Moons, T., Van Gool, L. J., Kempenaers, P., & Oosterlinck, A. (1995). Recognition of planar shapes under affine distortion. *International Journal of Computer Vision (IJCV)*, *14*(1), 49–65.

Pennec, X. (2006). Intrinsic statistics on Riemannian manifolds: Basic tools for geometric measurements. *Journal of Mathematical Imaging and Vision (JMIV)*, *25*(1), 127–154.

Polthier, K., & Schmies, M. (1998). Straightest geodesics on polyhedral surfaces. In *Mathematical visualization* (pp. 135–150). Heidelberg: Springer.

Qiu, H., & Hancock, E. R. (2007). Clustering and embedding using commute times. *IEEE Transactions on Pattern Analysis and Machine Intelligence*, *29*(11), 1873–1890.

Raviv, D., Bronstein, A. M., Bronstein, M. M., Kimmel, R., & Sochen, N. (2011a). Affine-invariant diffusion geometry of deformable 3D shapes. In *Proceedings of Computer Vision and Pattern Recognition (CVPR)*.

Raviv, D., Bronstein, A. M., Bronstein, M. M., Kimmel, R., & Sochen, N. (2011b). Affine-invariant geodesic geometry of deformable 3D shapes. *Computers & Graphics*, *35*(3), 692–697.

Raviv, D., Bronstein, A. M., Bronstein, M. M., Waisman, D., Sochen, N., & Kimmel, R. (2013). Equi-affine invariant geometry for shape analysis. Journal of Mathematical Imaging and Vision (JMIV).

Reuter, M., Rosas, H. D., & Fischl, B. (2010). Highly accurate inverse consistent registration: A robust approach. *Neuroimage*, *53*(4), 1181–1196.

Rugis, J., & Klette, R. (2006). A scale invariant surface curvature estimator, vol. 4319. In *Advances in Image and Video Technology, First Pacific Rim Symposium (PSIVT)* (pp. 138–147).

Rustamov, R. (2007). Laplace–Beltrami eigenfunctions for deformation invariant shape representation. In *Proceedings of Symposium on Geometry Processing (SGP)* (pp. 225–233).

Sapiro, G. (1993). *Affine Invariant Shape Evolutions*. PhD thesis, Technion-IIT.

Su, B. (1983). *Affine differential geometry*. Beijing: Science Press.

Sun, J., Ovsjanikov, M., & Guibas, L. J. (2009). *A concise and provably informative multi-scale signature based on heat diffusion*. In *Proceedings of Symposium on Geometry Processing (SGP)*.

Van Gool, L., Brill, M., Barrett, E., Moons, T., & Pauwels, E. J. (1992a). Semi-differential invariants for nonplanar curves. In J. Mundy & A. Zisserman (Eds.), *Geometric invariance in computer vision, chap. 11* (pp. 293–309). Cambridge, MA: MIT Press.

Van Gool, L., Moons, T., Pauwels, E. J., & Oosterlinck, A. (1992b). Semi-differential invariants. In A. Zisserman & J. Mundy (Eds.), *Geometric invariance in computer vision, Chap. 8*. Cambridge, MA: MIT Press.

Wang, Y., Gupta, M., Zhang, S., Wang, S., Gu, X., Samaras, D., et al. (2008). High resolution tracking of non-rigid motion of densely sampled 3D data using harmonic maps. *International Journal of Computer Vision (IJCV)*, *76*(3), 283–300.

Weiss, I. (1988). Projective invariants of shapes. Technical Report CARTR-339, Center for Automation, University of Maryland, January 1988.